TMPRSS2 activation of Omicron lineage Spike glycoproteins is regulated by TMPRSS2 cleavage of ACE2

Anupriya Aggarwal[1]*, Christina Fichter[1]*, Vanessa Milogiannakis[1]*, Anouschka Akerman[1], Timothy Ison[1], Mariana Ruiz Silva[1], Camille Esneau[2], Nathan Bartlett[2], Louise Burrell[3], Sheila Patel[3], Melissa Churchill[4], Thomas Angelovich[4], Rhys Parry[5], Julian D Sng[5], Greg Neely[6], Cesar Moreno[6], Lipin Loo[6], Anthony D Kelleher[1], Fabienne Brilot-Turville[7], Alexander Khromykh[5], Stuart G. Turville[1]

[1] The Kirby Institute, University of New South Wales, New South Wales, Australia.
[2] Hunter Medical Research Institute, University of Newcastle.
[3] Cardiovascular Research Group, The University of Melbourne, Parkville, Victoria, Australia.
[4] School of Health and Biomedical Sciences, RMIT University, Bundoora, Australia.
[5] School of Chemistry and Molecular Biosciences, Brisbane University of Queensland, Australia
[6] Charles Perkins Centre, Dr. John and Anne Chong Lab for Functional Genomics, Centenary Institute, and School of Life and Environmental Sciences, University of Sydney, Camperdown, New South Wales, Australia.
[7] Brain Autoimmunity Group, Kids Neuroscience Centre, The Children's Hospital at Westmead, Faculty of Medicine and Health, School of Medical Sciences, NSW, Australia.

*Equal primary author contribution

Abstract

Continued high levels spread of SARS-CoV-2 globally enabled accumulation of changes within the Spike glycoprotein, leading to resistance to neutralising antibodies and concomitant changes to entry requirements that increased viral transmission fitness. Herein, we demonstrate a significant change in ACE2 and TMPRSS2 use by primary SARS-CoV-2 isolates that occurred upon arrival of Omicron lineages. Mechanistically we show this shift to be a function of two distinct ACE2 pools based on cleavage or non-cleavage of ACE2 by TMPRSS2 activity. In engineered cells overexpressing ACE2 and TMPRSS2, ACE2 was cleaved by TMPRSS2 and this led to either augmentation or progressive attenuation of pre-Omicron and Omicron lineages, respectfully. In contrast, TMPRSS2 resistant ACE2 restored infectivity across all Omicron lineages through enabling ACE2 binding that facilitated TMPRSS2 spike activation. Therefore, our data support the tropism shift of Omicron lineages to be a function of evolution towards the use of uncleaved pools of ACE2 with the latter consistent with its role as a chaperone for many tissue specific amino acid transport proteins.

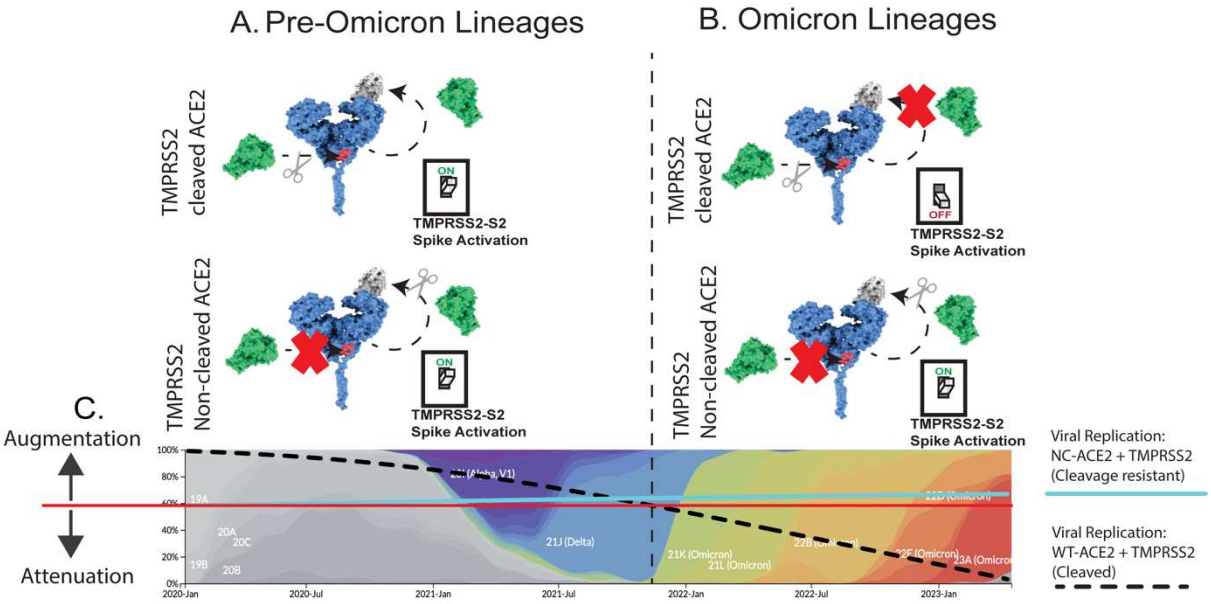

Graphical Abstract: Cleaved ACE2 pool model and evolution of SARS CoV-2 Tropism. **A. &B.** ACE2 cleaved pool model to reconcile the evolving entry requirements of SARS CoV-2 and changes in viral tropism *in vivo*. **A.** As observed for SARS CoV-1 and early SARS CoV-2 lineages, cleavage of ACE2 by TMPRSS2 augments cellular entry by enabling TMPRSS2 Spike S2 activation to proceed. In primary lower respiratory this would proceed to finely regulate ACE2 as part of the Renin Angiogensin System (RAAS). In other settings where ACE2 is not cleaved by TMPRSS2, entry still proceeds. In both ACE2 pools, TMPRSS2 activation can proceed ("on" conformation) **B.** For Omicron lineages, cleavage of ACE2 by TMPRSS2 is an "off" switch for latter TMPRSS2 Spike S2 activation. Whilst this supports attenuation in tissue where ACE2 is cleavage sensitive due to its role in RAAS (e.g. lung), replication in other tissue has been observed to proceed. Independent of RAAS, ACE2 can also act as a chaperone for several tissue specific amino acid transporters which engage at and around the TMPRSS2 cleavage site. To mimic lack of ACE2 cleavage in this setting, we mutated the ACE2-TMPRSS2 cleavage site and revealed settings where ACE2 is not subject to TMPRSS2 cleavage is a "on" switch for latter TMPRSS2 Spike S2 activation. **C.** Through

generating engineered lines that were biased for TMPRSS2 cleavage or expressed ACE2 that was TMPRSS2 resistant, we mapped the evolution of ACE2 and TMPRSS2 use across the first three years of the pandemic. In early clades, TMPRSS2 cleavage of ACE2 augmented ACE2/TMPRSS2 viral entry. This augmentation steadily decayed and led to attenuation upon the arrival of omicron BA.1 with continued attenuation observed now in XBB omicron lineages. Over the same time, TMPRSS2 cleavage resistant ACE2 has supported TMPRSS2 activation entry across all SARS CoV-2 lineages equally.

Introduction

Members of the coronaviridae family readily circulate within the human population with four common HCoVs (229E, OC43, NL63, and HKU1) known to cause mild to moderate upper-respiratory tract infections. In contrast SARS-CoV, MERS-CoV and SARS-CoV-2 are all associated with severe respiratory disease. Whilst the manifestation of clinical disease is complex and influenced by prior vaccine and convalescent immunity, a greater understanding of cellular entry pathways and viral tropism in coronaviruses is required to resolve the viral pathogenesis that eventually leads to clinical disease. Furthermore, many viruses, as they evolve, change how they target cells and tissue and this can in turn leads to different disease outcomes. Early clades of SARS CoV-2 had an entry pathway aligned with that of SARS CoV-1, where ACE2 was the primary receptor and fusion was activated by protease cleavage. The serine protease TMPRSS2 facilitated this at the membrane and the cysteine protease Cathepsin L within endosomes. Whilst the latter pathway is seen as a redundant mechanism of entry for the virus, murine knockout studies and *in vitro* infections, highlight the virus's preference for membrane entry mediated by TMPRSS2[3]. However, transmission and infection *in vivo* can take place across many tissues, with efficient entry into one tissue type often differing for another [4-7].

Early variants of concern (VOC) in the COVID-19 Pandemic followed a similar trajectory in tropism, with engagement of ACE2 with Spike S1 domain and then fusogenic activation through cleavage of S2 by TMPRSS2 [8,9]. The fitness gained by the first generation of variants of concern (Beta, Gamma and Alpha) has been primarily mediated by increases of ACE2 affinity through Spike polymorphisms such as N501Y [10,11]. With initial dominance of the VOC Alpha and then the appearance of the VOC Delta, key change at the furin cleavage site P681H and P681R led fitness gains primarily through efficient TMPRSS2 cleavage of S2. In brief, fusogenic activation of Spike required proteolytic cleavage of S at two distinct sites, S1/S2 and S2. Cleavage of subunits S1 and S2 occurred within producer cells through the action of Furin and both S1/S2 remained non-covalently linked. Whilst S1 subunit contains the receptor binding domain, S2 harbours the TMPRSS2 cleavage site, located immediately upstream of the hydrophobic fusion peptide and this triggers viral membrane fusion [8,12,13]. In a cell type dependent manner, prior cleavage of S1/S2 by furin increases the ability of S2 to access TMPRSS2 cleavage and this culminates in greater levels of viral fusion. Physiologically it was then observed that cell types with relatively high levels of TMPRSS2, including those from the lower respiratory tract, have augmented permissiveness to variants with efficient furin cleavage such as Delta [14-18].

The arrival of the initial BA.1 and BA.2 Omicron lineages shortly after Delta was a seismic shift at two levels. Firstly, the ability of Omicron lineages to efficiently evade neutralising antibodies, and secondly, a shift in tropism away from the lower respiratory tract [4-6,17-19]. This combination has driven waves globally that surpassed that prior to Delta. Whilst Omicron lineages have further diversified and in some cases recombined to create greater diversity, the fundamental understanding of the entry requirements of SARS CoV-2 is unclear at two levels. Firstly, the mechanistic basis of the tropic shift observed upon the arrival of Omicron BA.1/BA.2. Secondly, if continued evolution of the virus has maintained a Omicron entry pathway trajectory or alternatively is regressing back to the entry pathway observed at and prior to the VOC Delta. Herein, using genetically intact clinical isolates that span the pandemic to date we resolved viral replication across a continuum of engineered cells to resolve the entry requirements and/or restrictions across each variant. In doing so we define the Omicron tropic

shift to be a consequence of TMPRSS2-ACE2 proteolytic cleavage. For Pre-Omicron and Omicron lineages ACE2 proteolysis augments or attenuates TMPRSS2 spike activation respectively. This provides the mechanistic basis of the change in viral tropism upon the arrival of Omicron and reconciles discrepant *in vitro* and *in vivo* observations of TMPRSS2 spike activation through the alignment of this activation with two distinct ACE2 pools. The first ACE2 pool in a conformation sensitive to TMPRSS2 proteolysis and second pool in a conformation that is resistant.

Results

Cell lines expressing ACE2 and TMPRSS2 reveal a continuum of sensitivity across all major primary SARS CoV-2 variants

Throughout the pandemic, we have worked alongside genomics surveillance units to enable isolation and study of primary SARS CoV-2 isolates. Early in the pandemic, both ourselves and others engineered cell lines to enable isolation and testing of primary isolates in real-time [19-22] This primarily was enabled by emulating the entry pathway known in primary cells and *in vivo*, through expression of the primary receptor ACE2 and the surface expressed serine protease TMPRSS2, a well-known protease present at high levels in the lung, prostate, liver and gastrointestinal tract. Hek 293T and VeroE6 have been extensively used in virological assays, as they lack key innate immune mechanisms and as such represent pragmatic cell substrates for assay platform development and also viral propagation [19-22]. At the juncture of the Delta to Omicron BA.1 shift in the pandemic, both ourselves and others struggled to isolate and maintain primary viral isolates in a manner similar to what we had observed prior to BA.1, as in many cases the ACE2-TMPRSS2 pathway that previously was functional for early variants, appeared no longer functional for Omicron lineages [17,19,23-25]. To increase the efficiency of primary isolations from nasopharyngeal swabs, we screened existing cell lines across primary isolates encompassing the major variants that have appeared over the last three years globally (Fig. 1A). Rather than manually score viral titers, we used a high throughput imaging approach with live cell nucleus staining that can enumerate the accumulation of viral cytopathic effects through the dose dependent loss of nuclei [19,22] (Fig. 1B). Combined with automated nuclei counting algorithms, this provided a non-biased pragmatic means of screening variant panels against many cell lines. Using this approach, we observed a continuum of sensitivities to evolving variants (Fig. 1 C-G). As expected, the VeroE6 line was the least permissive, whilst all TMPRSS2-expressing cell lines sustained greater viral titers (Fig. 1 C-G). Whilst all TMPRSS2-expressing cells were sensitive to Delta, only one Vero cell clone expressing TMPRSS2 (VeroE6-T2) was sensitive across all variants (Fig. 1F). Curiously an equivalent VeroE6 cell line (VeroE6-T1) generated titers ten-fold lower than this latter cell line (Fig. 1E versus 1F). Subsequent viral expansions using the VeroE6-T2 line also revealed that RNA copies/ml of virus generated over 24 hours were high across all variants (5.08×10^8 copies/ml +/- 2.74×10^8; IQR 2.89×10^8; Supplementary table I) tested. The HAT-24 Hek based line then the second VeroE6 TMPRSS2 line (VeroE6-T1) were ranked the next sensitive across all variants. In general, for infectivity to particle ratios, the latter cell line observed slight attenuation across all Omicron lineages. To anchor these observations with other studies and also an non-engineered cell line closer to that of lung tissue *in vivo*, we subsequently tested all variants across the Calu3 cell line, which is a Human Lung Adenocarcinoma derived Cell Line. Calu3 infections resulted in profiles to the Vero-E6-T1 line with the exception of clear attenuation in the majority of Omicron lineages. To further resolve the entry requirements and basis of the susceptibility of the VeroE6-T2 cell line alongside the other cells tested, we stained cells for the SARS CoV-2 entry factors TMPRSS2 (Fig. 1I) and ACE2 (Fig. 1J). We observed the VeroE6-T2 line to express the highest levels of TMPRSS2 and low levels of ACE2 but at levels similar to that observed in the VeroE6-T1 line. Whilst TMPRSS2 levels are higher in the VeroE6-T2, high expression of TMPRSS2 is inconsistent with that observed in previous studies, where TMPRSS2 levels were associated with high levels of Omicron attenuation [24]. Therefore other mechanisms, in addition to ACE2 and TMPRSS2 expression, are rescuing replication in Omicron lineages in the VeroE6-T2 line.

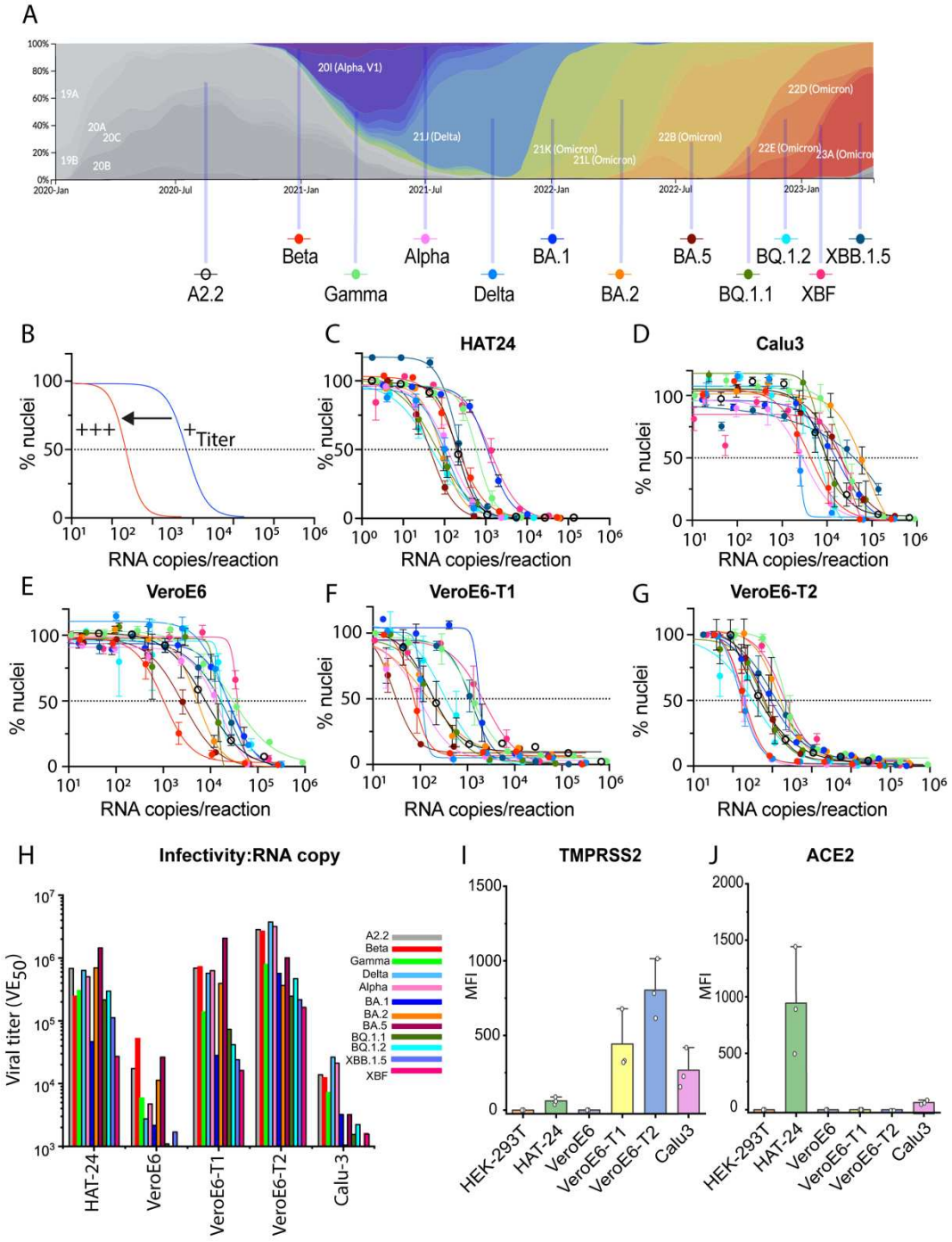

Figure 1. Engineered lines with TMPRSS2 reveal a continuum of sensitivity across all major primary SARS CoV-2 variants

A. Frequency of SARS CoV-2 variants coloured by Clade (nextstrain.org/sars-cov-2). Below are the primary isolates used in this study and throughout the pandemic represent either variants of concern and/or dominant variants in the community at that time. **B.** Schematic of high content datasets when RNA input is known. Shifts of the sigmoidal shifts to the left represent greater titers for that isolate, as cytopathic effects sustained at lower viral input can be readily enumerated in high content microscopy using live fluorescent nuclei counts. The dotted line represents 50% loss of nuclei and interpolated values can be used as surrogates for viral titers. **C-G.** Titration curves per RNA input for primary clinical isolates highlighted in A. **C.** Is the Hek-293T cell line coexpressing ACE2 and TMPRSS2 as previously described [19]. **D.** Calu-3 Human Lung Adenocarcinoma Cell Line. **E.** Is a parental VeroE6 line. **F.** A VeroE6 line expressing TMPRSS2 as previously described[20]. Herein we refer to this line as VeroE6-T1. **G.** Another VeroE6 line expressing TMPRSS2 as previously described [21]. Herein we refer to this line as VeroE6-T2. G. **H.** Infectivity to RNA ratios. Infectivity is calculated by the viral dilution requited to sustain 50% of the loss of nuclei (interpolated from the dose dependent sigmoidal curve fit). RNA copies are detected and calculated as previously described[26]. I &J. Cell surface staining and Flow cytometry of cells used herein for **I.** TMPRSS2. and **J.** ACE2. Note the VeroE6-T2 line expresses the highest TMPRSS2 levels. Each point represents independent experiments. Data from C. to G. are representative plots of three independent experiments. Each point and standard deviation represent the mean and variation across 4 technical replicates. Infectivity to RNA ratios are derived from data generated from C. to G. and is representative of three independent experiments.

High ACE2 expression in the presence of high TMPRSS2 augments pre-Omicron lineages and attenuates Omicron lineages

To confirm that entry with the VeroE6-T2 line was primarily mediated by TMPRSS2 spike activation, we titrated virus with the TMPRSS2 inhibitor Nafamostat. Using this approach, we observed significant decreased sensitivity of this cell line upon treatment across all variants (Fig. 2. A-D). Whilst treatment with the Cathepsin L inhibitor E64D blocked entry into the parental VeroE6 line using two variants that represent pre-Omicron and Omicron lineages (Fig. S1A), we did not observe inhibition of entry with E64D in the VeroE6-T2 line (Fig. S1B). Therefore, in contrast to other studies [24] using engineered cell lines, TMPRSS2 spike activation was still functional in this cell line and as such enabled isolation and replication across pre-Omicron and Omicron lineages. In an attempt, to resolve the contrasting observations herein and elsewhere, we increased ACE2 expression on the VeroE6-T2 line (Fig. 2E) to determine if this would further augment viral replication across variants. Subsequent testing of this cell clone across all variants did observe augmented infection for all pre-Omicron lineages and especially Delta, but in contrast, high levels of attenuation across all omicron lineages (Fig. 2F-I). This was consistent with that observed for the Calu3 cell line, but with far greater changes observed between titers of pre-omicron and omicron lineages. For the VeroE6-T2-ACE2 cell line we could readily group attenuation with earlier omicron lineages circulating in 2022 subject to less attenuation than that observed by the more contemporary 2023 recombinants XBF and XBB.1.5 (Fig. 2I). Paradoxically, these two latter isolates have the highest level of ACE2 affinity as they both have the F486P Spike polymorphism, and this is supported to enable their fitness in transmission [27]. To confirm the relative affinities of ACE2 within these two primary isolates versus other contemporary Omicron lineages, we developed an ACE2 inducible line without TMPRSS2 to determine the efficiency of use by these two latter emerging variants with reported high ACE2 affinities. This line we refer to as the ACE2 Affinofile line as it uses a similar approach to that outline by Lee and colleagues for HIV-1 [28]. Whilst entry into this cell line with limiting ACE2 expression would confirm the observation of high ACE2 affinity, it would also control for attenuation of viral entry through a TMPRSS2 independent pathway. For this we tested the two known high ACE2 affinity isolates, XBB.1.5 and XBF versus two low ACE2 affinity isolates, XBB.1 and CH.1.1. and observed efficient ACE2 [29] usage by primary isolates but furthermore found that both XBF and XBB.1.5 can readily infect cells with high ACE2 expression in the absence of TMPRSS2 expression (Fig. 2J &K). This contrasts directly with what is observed in the VeroE6-T2-ACE2 line expressing high ACE2 and therefore supports attenuation in this latter cell line to be primarily related to regulation of TMPRSS2 spike activation following ACE2 engagement.

TMPRSS2-cleaved ACE2 augments TMPRSS2 usage by pre-Omicron variants but attenuates Omicron sub-lineages

Unlike other viral receptors, ACE2 is physiologically important in two distinct pathways. The first relates to ACE2's carboxypeptidase activity and the need to cycle from membrane bound to soluble forms to regulate the renin-angiotensin-aldosterone system (RAAS), a critical regulator of blood volume, electrolyte balance, and systemic vascular resistance *in vivo* [30]. In the setting of ACE2's role in RAAS, ADAM17 and TMPRSS2 regulate the shedding and retention respectively through differential ACE2 cleavage in the exposed neck of ACE2. The second physiological role occupies the largest pool of ACE2 in as a dimer of heterodimers when acting as a chaperone with one of two known solute carrier proteins, SLCA619 and SLCA620. Whilst it is known that viral entry through ACE2 is separable from its enzymatic

activity [8], ACE2 cleavage by TMPRSS2 has been observed to augment viral entry for the

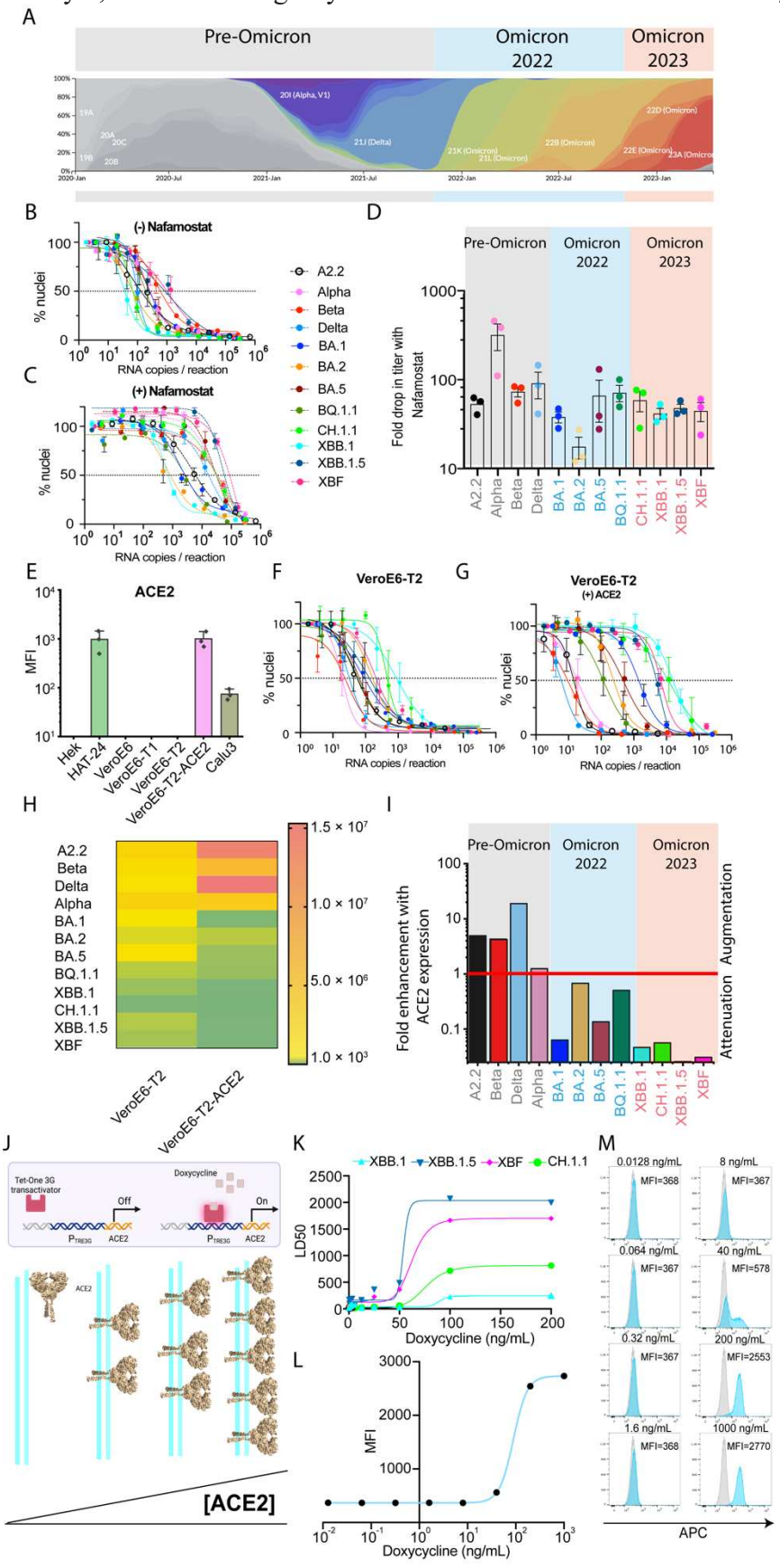

Figure 2. High co-expression of ACE2 and TMPRSS2 attenuates Omicron lineage use of TMPRSS2

A. Frequency of SARS CoV-2 variants coloured by Clade (nextstrain.org/sars-cov-2) over the pandemic. Three periods of variants spread are highlighted by shading in grey (Pre-Omicron), blue (2022 Omicron) and pink (2023 Omicron). **B. & C.** Viral titrations in the **B.** absence or **C.** Shifts of titration curves from the right to the left show reduced titers and provide a quantitative measure of TMPRSS2 dependence for entry in the VeroE6-T2 cell line. **D.** Summary of fold reduction in titers in the presence of Nafamostat. Each variant period is shaded in grey, blue and pink to align with variant periods outlined in **A.** Whilst initially pre-Omicron lineage titers are highly dependent on TMPRSS2, there is a significant drop observed with the arrival of Omicron BA.1 and BA.2. Whilst there is a drop in TMPRSS2 use, all variants were observed to have greater than ten-fold increase in titers in the absence of Nafamostat. **E.** Surface expression of ACE2 in the VeroE6-J2-ACE2 cell line relative to other cell lines presented in figure 1. **F & G.** Viral titers in the VeroE6-T2 cell line **F.** without and **G.** with high ACE2 expression. Left and right shifts in the sigmoidal curves is evidence for attenuation and augmentation respectively. **H.** Summary of titers in the VeroE6-T2 line with and without ACE2 overexpression. Note pre-Omicron titers can be readily observed to be augmented in the high ACE2 and high TMPRSS2 setting. **I.** Shading of variant eras as per **A.** Ratios of titers in VeroE6-T2-ACE2 to its parent VeroE6-T2 establish levels of augmentation or attenuation. The red line is where titers are equivalent in each cell, whilst above the red line variants are augmented and below the red line variants are attenuated. **J.** ACE2 Affinofile cell line. In brief, the Hek-239T cell line was engineered to express variable levels of ACE2 using a Doxycyline sensitive promoter. The greater the [Doxycyline], the higher the expression of ACE2. **K.** Viral titers for XBB.1, XBF, XBB.1.5 and CH.1.1. The F486P polymorphism in XBF and XBB.1.5 increases ACE2 affinity. **L & M.** Summary of ACE2 expression with increasing Doxycycline.

related virus SARS CoV-1 [31]. To investigate the dynamics of ACE2 and TMPRSS2 in SARS CoV-2 entry, we turned to the continuum of cell lines we engineered to determine if shedding or retention of ACE2 was associated with augmented or attenuated viral replication across a range of clinical isolates that spanned the pandemic. Across all engineered cell lines, from the parent VeroE6, VeroE6-T1, VeroE6-T2, VeroE6-T2-ACE2 and HEK 293 ACE2/TMPRSS2, we detected activity for soluble ACE2. The only cell line to record undetectable soluble ACE2 was the Veroe6-T2-ACE2 line, the cell that is observed with the greatest levels of ACE2 & TMPRSS2 co-expression (Fig. 3A& B). In contrast the HEK 293 cell line expressing similarly high levels of ACE2 but low levels of TMPRSS2 was the cell line with the highest level of soluble ACE2 (Fig. 3A&B). Thus, these observations are consistent with previous studies that highlight TMPRSS2 competes with other proteases to cleave ACE2 in a manner that impedes subsequent release of soluble ACE2 [31]. Whilst TMPRSS2 can cleave ACE2, it does not lead to increased levels of soluble ACE2 but rather promotes retention of ACE2 as a membrane bound cleaved form [31]**.** Given the above observations and the prior observations that ACE2 cleavage by TMPRSS2 can contribute to SARS-CoV-1 entry [31], we generated a cleavage resistant mutant (Fig. 3C) as previously described [31] and overexpressed this at similar levels within the VeroE6-T2 line (Fig. S2). Across all variants, we then tested the VeroE6-T2 line with and without ACE2 bearing the TMPRSS2 cleavage site (NC-ACE2). Here we observed lower levels of augmentation of pre-Omicron variants, with the largest drop observed in the earliest circulating Clade A variant and thus consistent with a mechanism of SARS-CoV-1 augmented entry when TMPRSS2 cleaves ACE2 [31]. In contrast the removal of the TMPRSS2 cleavage site in ACE2 rescued all Omicron lineages and as such all major SARS-CoV-2 isolates across the pandemic maintained replication at similar levels (Fig. 3D). Analysis of other clones with marginally lower levels of NC-ACE2 expression, revealed the same phenotype (Fig. 3F) across all variants but with lower levels of infectivity across all lineages. To determine if the NC-ACE2 phenotype could be reproduced in another cellular setting, we generated a Hek-239T line with only NC-ACE2 and co-expressed TMPRSS2. To consolidate testing, we investigated the pre-Omicron clade A2.2 versus the contemporary XBB.1.5 omicron lineage. For the NC-ACE2 phenotype to be reproduced, equivalent permissiveness to both clades (one that emerged in 2020 and the other in 2023) should proceed and this was observed (Fig. 3N). Therefore, we conclude TMPRSS2 cleavage-resistant ACE2 can sustain replication of all SARS CoV-2 variants tested at equivalent levels, whereas TMPRSS2 cleaved ACE2 (WT ACE2 expressed alongside high TMPRSS2) only provides an entry advantage for early pre-Omicron variants. As Omicron (XBB.1.5) cultures of cleavage-resistant ACE2 were observed to accumulate syncytia in a similar manner to Delta in the WT ACE2-TMPRSS2 setting (Fig. 3I. &3J), we hypothesised that TMPRSS2 cleavage of ACE2 was a switch that blocked subsequent

TMPRSS2 Omicron Spike S2 activation. To test this, we titrated virus in the presence and absence of Nafamostat using the NC-ACE2 VeroE6-T2 line. Following treatment we observed large shifts in viral titer curves, with all Omicron lineages shifting approximately 100-fold lower in titer (Fig3. K & L). This observations supports efficient TMPRSS2 spike activation across all SARS CoV-2 variants when the engage TMPRSS2 resistant ACE2. So here we conclude that TMPRSS2 cleavage of ACE2 acts as an "off" switch for subsequent TMPRSS2 activation of Omicron Spikes. Whereas the "on" switch is maintained by ACE2 pools that are TMPRSS2 resistant. In contrast, the "on" switch of TMPRSS2 activation is sustained in both ACE2 pools for pre-Omicrons and actually augmented when ACE2 is cleaved.

Given high levels of TMPRSS2 expression are associated with Omicron attenuation in previous studies [24], we then tested the hypothesis that ratios of ACE2 to TMPRSS2 was the primary driving force behind enrichment of TMPRSS2 cleaved ACE2. Physiologically, this may explain partially why attenuation proceeds in the lung, given the high levels of expression in that tissue over the upper respiratory tract [24]. To test if ratios of ACE2 to TMPRSS2 defined the biasing of ACE2 pools, we turned to our Doxycycline induced ACE2 expression model in the presence of TMPRSS2 to test this. For this we consolidated to a pre-Omicron (Clade A.2.2) versus the most contemporary Omicron variant XBB.1.5. Using this approach, we observed increasing levels of infection for the pre-Omicron clade A2.2 associated with increasing ACE2 levels in the presence of TMPRSS2, but significantly limited replication for XBB.1.5 at all Doxycycline/ACE2 concentrations (Fig. 2M). Therefore, we conclude that in the presence of TMPRSS2, ACE2 expressed alone is susceptible to TMPRSS2 cleavage across a range of densities.

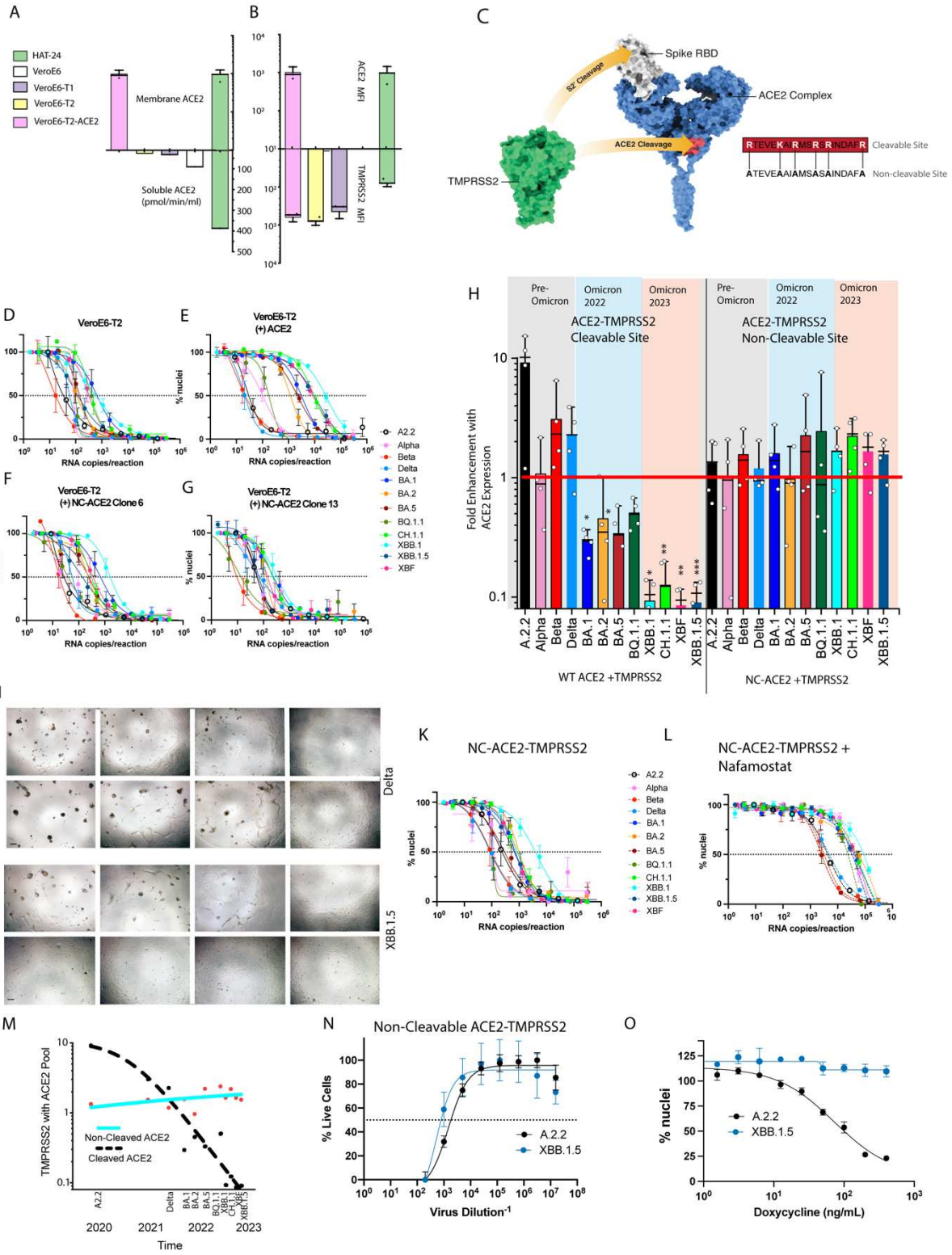

Figure 3. TMPRSS2 cleavage of ACE2 resolves the entry differential entry requirements for pre-Omicron and Omicron lineages.

A. Membrane and soluble ACE2 levels in engineered cell lines. Membrane ACE2 is detected through flow cytometry and represented as mean fluorescence intensity. The activity of soluble ACE2 is detected using the supernatant of 80% confluent cell lines after three days of culture as previously described [1]. **B.** Ratios of cell surface ACE2 and TMPRSS2 detected via flow cytometry as per A. are presented as a comparison. **C.** Schematic of Spike (Grey), TMPRSS2 (blue) and ACE2 (yellow) are presented on the left. On the right is the ACE2 structure with the TMPRSS2 cleavage site in red (Structure PDB 6M17; [2]), with the TMPRSS2 amino acid cleavage boxed in red and the sequence of the ACE2 TMPRSS2 resistant mutant to the right in black with alanine substitutions in bold. D.-G. Viral titration curves with **D.** low WT ACE2:High TMPRSS2 **E.** High WT ACE2:High TMPRSS2. Input viral inocula is presented here in RNA copies per infection/reaction. **F.** High NC mutant- ACE2: High TMPRSS2 (clone 6 wit
h lower NC-ACE2 expression). **G.** High NC mutant- ACE2: High TMPRSS2 (clone 13 with high NC-ACE2 expression relative to clone 6). **H.** Summary of Fold Augmentation and attenuation compared to the low WT ACE2:TMPRSS2 cell line presented in D. In the Left panel is the fold change in titers using the high WT ACE2: high TMPRSS2 presented in E. On the right panel is the fold change in titers for the NC ACE2 mutant clone 13 presented in panel G. above the red line represents augmentation and below the red line attenuation. **I-J.** Contrasting cytopathic effects appearing in WT ACE2: TMPRSS2 high and NC ACE2: TMPRSS2 high VeroE6 lines presented in E. and G. respectfully for pre-Omicron lineage Delta and the Omicron lineage XBB.1.5. Fields of view from left to right are starting at 1/2000 dilution with 1/5 dilution steps in each successive frame. Note the Omicron lineage XBB.1.5 leads to extensive viral syncytia formation only in the presence of NC ACE2. Whilst for pre-Omicron Delta, syncytia proceed at a similar level across WT and NC engineered cell lines. Scale bar is at 20um. **K & L.** Using the cell clone presented in G. we tittered virus in the K. absence or L. presence of saturating levels of the TMPRSS2 inhibitor Nafamostat. With data presented as input RNA copies of virus per variant, sigmoidal curve shifts to the left in K. to the right in L. demonstrate the lower levels of viral titers as TMPRSS2 use is lost. M. ACE2:TMPRSS2 ratios cannot recapitulate the TMPRSS2 cleavage resistant phenotype. Here, the cell clone presented in Fig.2 J has been engineered to also express TMPRSS2. Through the use of Doxycycline, ACE2 expression is increased in a dose dependent manner. **N.** Expression of NC-ACE2 in a Hek293T line co-expressing TMPRSS2. Titers curves of A2.2 and XBB.1.5 are used here as controls to recapitulate the data initially observed in VeroE6 lines presented in H. and K. **O.** The use of cleavage sensitive ACE2 and NC ACE2 in the presence of TMPRSS2 is presented across the pandemic to date. The Y-axis is change in titers upon over-expression of WT ACE2 or NC-ACE2 in the presence of high TMPRSS2. >1 represents augmentation, <1 represents attenuation. Of note, all emerging lineages have become increasingly attenuated in the presence of high WT ACE2-TMPRSS2 co-expression. *p<0.05, **p<0.01, ***p<0.001.

Pools of ACE2 *in vivo* that potentially resolve evolving tropism of SARS CoV-2 variants

In removing the ability of TMPRSS2 to cleave ACE2, we have resolved a switch mechanism between ACE2 and TMPRSS2 that either blocks or enables Omicron S2 spike activation by TMPRSS2 use. The continued use of TMPRSS2 by Omicrons can explain the observed discrepancies of use of TMPRSS2 by Omicrons *in vivo* versus that observed *in vitro* by ourselves and others, as overexpression of ACE2 and TMPRSS2 in cells lines can simply result in biasing of cells towards cleaved ACE2 pools. Key to further resolving Omicron tropism *in vivo* is fundamentally understanding the two very separate roles ACE2 has *in vivo* and how this potentially relates to Omicron tropism. The first well known role for ACE2 is the regulation of soluble ACE2 in the renin angiotensin system which requires ACE2 proteolytic cleavage events to proceed[30] . Whilst the renin angiotensin system and the role of ACE2 in the lung are well known, the majority of ACE2 within the body is related to its role as a chaperone of a number of solute carrier proteins. Further evidence that solute carrier protein can influence infection is based on bidirectional CRISPR screens, where activation of expression of SLC6A19 was observed to positively influence SARS CoV-2 infection in the lung derived Calu3 cell line. Whereas the SLC6A20, whose structure has also been solved in a quaternary complex with ACE2 [32], has been linked to the gene cluster locus 3p21.31 [33] to be associated with Covid severity in GWAS studies. We would support TMPRSS2 resistant ACE2 in its chaperone role for three underlying reasons. Firstly, the solute carrier form dimers of heterodimers with ACE2 and in doing so the TMPRSS2 cleavage site is structurally occupied at the ACE2 dimer interface (ACE2 amino acid residues 710 and residue 716). Secondly, mechanistically ACE2 in its role as a chaperone, would need to not only remain membrane bound but also would not benefit from the proteolytic regulation via TMPRSS2. Finally modelling studies of ACE2 dimers complexed with SLC6A19, reveals TMPRSS2 is obstructed from accessing the known cleavage site [34].

Given the structure of ACE2 in its role as a chaperone for solute protein carriers had the potential to rescue Omicron infection, we then investigated the expression of SLC6A19 and SLC6A20 across the targets of SARS CoV-2 throughout the body to resolve their potential in

driving SARS CoV-2 tropism *in vivo*. For this we analysed single cell data for the nasal cavity, the lung and ileum as major SARS CoV-2 *in vivo* reservoirs. To resolve each *in vivo* target population we resolved the ratios of ACE2 and TMPRSS2, alongside SLC6A19 and SLC6A20. Ciliated nasal epithelial cells (HNCs) expressed low levels of ACE2 and was associated with low SLC6A20 expression and moderate TMPRSS2 expression. In the lung TMPRSS2 dominated expression over ACE2 and SLC6A20 in type I & II pneumocytes (Fig.4. C., D. and H.). In contrast, if we look at entry factors in enterocytes of the ileum, ACE2 and SLC6A19 are expressed at equivalent high levels, with TMPRSS2 levels lower than that observed in lung pneumocytes (Fig. 4. E., F. & I.). As in other tissues, SLC6A20 was also present at low levels within known SARS CoV-2 targets. Therefore, *in vivo* the lung and the lower intestine represent tissue sites that represent the two differing compartments and functions of ACE2: i.e. RAAS and regulation of soluble ACE2 in the lung and SLC6A19 chaperone function in the intestine.

Waste Water SARS CoV-2 viral loads support infection of the Ileum to remain constant across the pandemic.

In animal models and primary cultures, it is well documented that Omicron lineages are attenuated and TMPRSS2 cleavage of ACE2 switching "off" latter TMPRSS2 spike activation is consistent with the observations of Omicron entry requirements herein [4]. Given ACE2's differing role as chaperone in the intestine, we looked to determine if Omicron lineages were attenuated in a manner similar to the lung. If the latter were the case, then we would conclude that the ACE2 pool in that tissue is subject to equivalent TMPRSS2 cleavage. In contrast if there was no evidence of attenuation, we would then conclude the ACE2 in its chaperone function is not subject to TMPRSS2 cleavage and as such can sustain replication of all SARS CoV-2 lineages. Rather than obtaining primary enterocytes and determining replication across SARS CoV-2 variants, we turned to an epidemiological approach using the signal of SARS CoV-2 in Waste-Water (WW) in the US population over time. Combined with high levels of genomic surveillances and diagnostic testing, WW viral loads/ml can then be correlated with actual reported cases across variant specific waves like Delta and Omicron BA.1. To test this latter hypothesis, we obtained the average WW viral load signal across the pandemic in the US and then plotted this against reported case numbers. Given cases are often under-reported, we looked at another surrogate for case-loads in the community. Anti-nucleocaspid antibodies only appear in individuals following infection and have been used prior in serosurveillance studies [35]. Throughout the pandemic IgG pooling and purification is used in the manufacture of 10% IgG IVIG) for clinical use in conditions such as replacement therapy for primary and secondary immunodeficiencies. Each batch consists of IgG purified and pooled from in excess of 10,000 US based plasma donations collected over the period of approximately one month. As an alternate surrogate measurement of case-loads, we determine the levels of anti-Nucleocapsid antibodies in each batch per month for alignment with that observed in WW signals. Ratios for Omicron:Delta for reported cases at the peak of each wave was 6.51. In comparison WW ratios were 5.97 and IVIG anti-nucleocapsid IgG was 3.82. Whilst IVIG ratios were lower than reported cases, similar ratios were obtained for WW viral loads and as readily concluded in Biobot WW datasets (https://biobot.io/why-wastewater-was-a-leading-indicator-of-the-omicron-surge/). Therefore, WW viral load does not support attenuation of the viral load from intestinal shedding following the arrival of Omicron and this supports continued replication in this tissue reservoir.

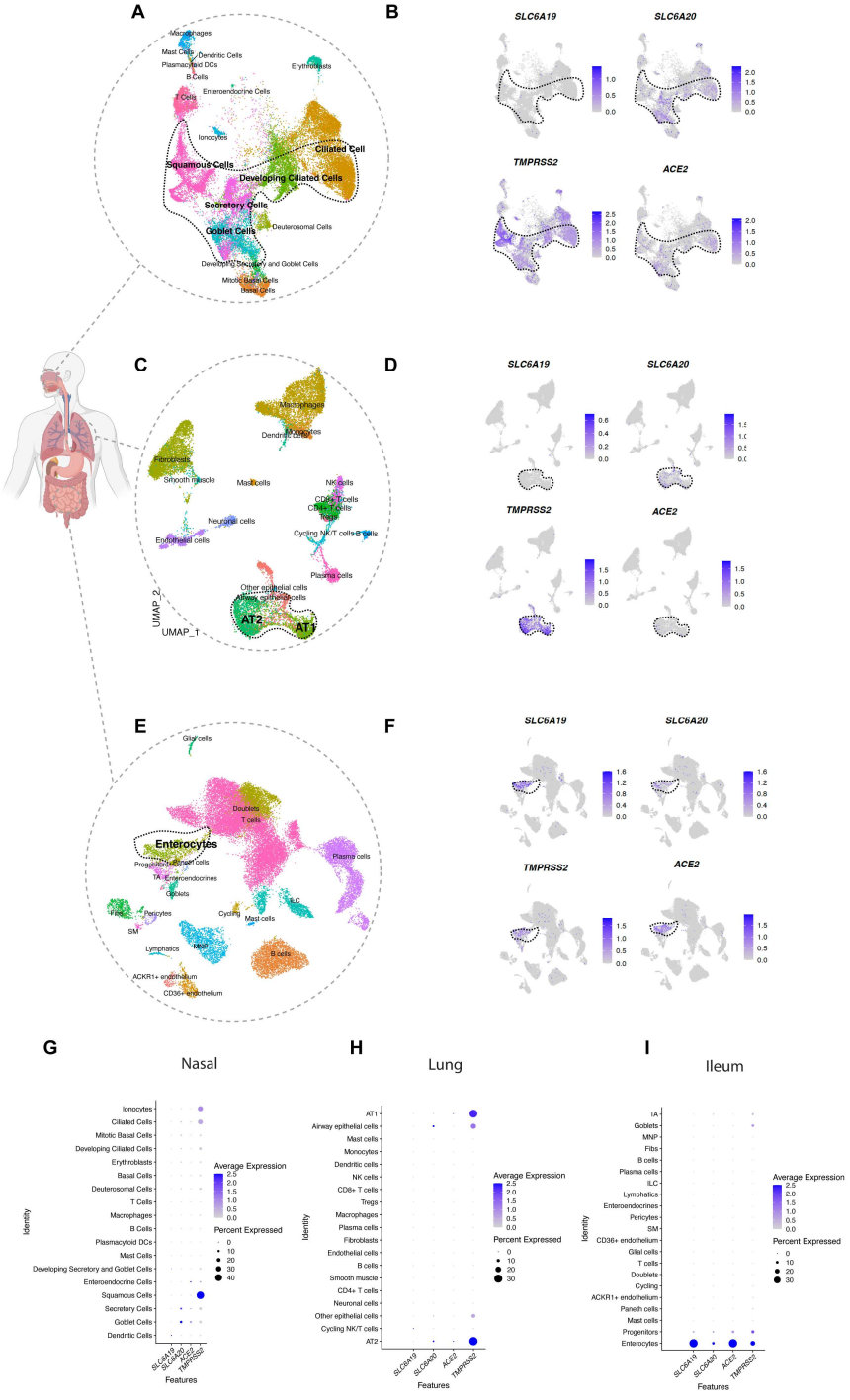

Figure 4. Expression of known SARS CoV-2 viral receptors with solute protein carriers SLC6A19 and SLC6A20 in targets of the nasal epithelium, lung and lower intestine. **A.-F.** Uniform manifold approximation and projection (UMAP) of **A.** Nasal Epithelia. **C.** Lung and **E.** Small intestine using single nuclei RNA sequencing. Cell types are color-coded. Target cells within each tissue are highlighted in B. D. & F. in respective tissues, with expression of protein solute carriers SLC6A19 and SLC6A20 alongside the known SARS CoV-2 receptors ACE2 and TMPRSS2. In **G.** to **I.** Relative expression of each solute carrier with ACE2 & TMPRSS2 is presented for each major cell type resolved in each tissue.

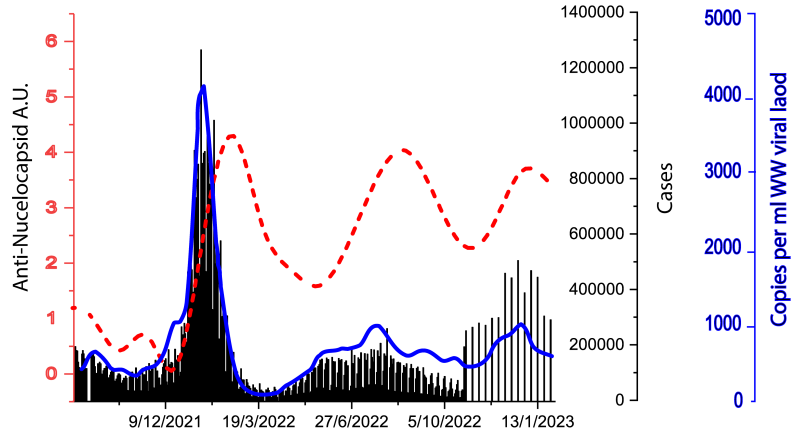

Figure 5. Reported case numbers, IVIG anti-nucleocapsid IgG and waste-water viral loads across variant waves. Waste water viral load per ml is presented (blue) alongside reported cases (black histograms) and antinucleocapsid IgG in pooled antibodies from approximately 720,000 US plasma donors (red). Of note, following the Delta to Omicron shift, reported cases and anti-nucleocapsid content in IVIG are of similar magnitude to that observed in wasted water viral loads. Thus supporting lack of any observed attenuation in tissue contributing to the waste water viral load at the time Omicron BA.12 emerged.

Discussion

Resolution of viral entry pathways is essential for not only the tracking the fitness of viral variants and their ability to spread, but importantly gives further insight into the pathogenesis and potential clinical manifestations as it appears in the community. Whilst in most instances, the shifts in viral entry are subtle, there are occasions where significant accumulation of changes in a viral glycoprotein can enable a seismic shift in how the virus engages and infects cells and tissues. For SARS-CoV-2, whilst the majority of cases infections are rapidly cleared and accumulated genetic changes can be minor, chronic infections can occur and have been observed in immunocompromised patients [36-39]. This accumulation and then appearance of variants within the community is the primary hypothesis for the appearance of early variants of concern and in the case of the appearance of early Omicron lineages [38]. As with other chronic viral infections, SARS-CoV-2 evolved to target cells and tissues in a manner different from earlier circulating variants. From preliminary studies by ourselves and others, it was immediately apparent that Omicron lineages were engaging the serine protease TMPRSS2 in a manner that differed from Delta and variants that spread prior to Delta [19,24,40]. This change in entry manifested *in vivo* in animal models [4] and also in clinical observations to either observe lack of targeting within the lung and reduction of Covid-19 associated pneumonia [41]. Herein using extensive panels of genetically intact primary isolates that covered the pandemic from early 2020 through to early 2023, we mechanistically dissected the evolving entry requirements for SARS variants across the pandemic to date. Using this approach, we observed the major shift in entry requirements from Delta to Omicron lineages is the culmination of TMPRSS2 activity on both ACE2 and SARS CoV-2 Spike activation. If the TMPRSS2 site of ACE2 is available for subsequent cleavage, then latter activation of Omicron Spike by TMPRSS2 does not proceed (Cleaved ACE2 is in the “off” conformation to enable TMPRSS2 Omicron Spike activation). In contrast pre-Omicrons are augmented under the same entry conditions and engage TMPRSS2 irrespective of ACE2 cleavage conformations.

The phenotypic shift from Delta to Omicron has been studied extensively and the changing requirements for entry have been documented and supported at many levels. Omicron entry hypothesis is broadly based on the inefficient cleavage of the S1/S2 Spike domains, as in the setting of uncleaved S1/S2, fusogenic activation of S2 by TMPRSS2 is reduced and endosomal

entry pathways increased. In the endosomal entry pathway, Spike utilises the cysteine protease Cathepsin L to activated and drive S2 fusion across the endosomal membrane [24,40] and this does not require prior S1/S2 Spike cleavage by Furin. Whilst observations of Omicron BA.1 do support this hypothesis, the emergence of a number of Omicron lineages post BA.1 have observed a continuum of S1/S2 cleavage [42,43] but to date an entry phenotype not consistent with that observed for pre-Omicron lineages such as Delta. For many *in vitro* studies, we readily support and independently confirm that Omicron lineages may indeed be forced into using the endosomal pathway in setting where TMPRSS2 spike activation is attenuated/switched off. Whilst TMPRSS2 independent entry through endocytosis is a well-documented pathway *in vitro*, accumulating evidence *in vivo* supports continued use of TMPRSS2 as a dominant entry pathway required for viral replication and persistence on Omicron lineages [3,44]. In addition, give the fitness gain of the virus using TMPRSS2, continued use of this serine protease for efficient viral entry is consistent with its high transmissibility *in vivo*. Here we support the major shift in the Omicron entry is the condition at the plasma membrane which drives TMPRSS2-ACE2 cleavage subsequently drives attenuation of TMPRSS2 spike activation across Omicron lineages. Following the resolution of entry requirements by a continuum of primary SARS CoV-2 isolates that span the pandemic, we propose the following "TMPRSS2 cleaved ACE2 pool" model for the change in viral entry requirement observed for Omicron lineages versus pre-Omicron lineages. In this model under conditions that drive TMPRSS2-ACE2 cleavage, there is augmentation of pre-Omicron lineages but progressive attenuation of Omicron lineages spanning from BA.1 to the more contemporary XBB.1.5. The physiological relevance to the above proposed model is consistent with the pools of ACE2 needed for the RAAS pathway (cleavage sensitive) versus pools of ACE2 that either play a chaperone role for many solute protein carrier proteins or are not sustained in a conformation that enables TMPRSS2 cleavage (cleavage resistant pools). With respect to support for ACE2's chaperone role being TMPRSS2 cleavage resistance, molecular docking studies of ACE2 complexed to the solute carrier protein SLC6A19 observed lack of TMPRSS2 access to the TMPRSS2-ACE2 cut site [34] and this is consistent with engagement of the cut site within the ACE2 dimer interface when ACE2 is functioning as a protein solute carrier chaperone. Whilst SLC6A19 expression is enriched in the gut, the solute SLC6A20 is observed across all known SARS CoV-2 primary tissue targets, ranging from the upper respiratory tract, lung, small intestine and brain (chloroid plexus) [45-47] highlighting a continuum of ACE2 chaperone roles across many tissues associated with SARS CoV-2 infection [33,48-51]. Bidirectional CRISPR screens in the Lung derived Calu3 cell line also highlight how SLC6A19 can influence SARS CoV-2 infection [48]. In these latter studies, only cell lines with TMPRSS2 activity were observed to influence infection following SLC6A19 CRISPR activation. Importantly, the dominant role of ACE2 in the ileum is as a chaperone with SLC6A19 and WW viral load data over time supports infection of this tissue to be unchanged by the arrival of Omicron, and from the mechanisms outlined herein we would readily support this ACE2 pool to be resistant to TMPRSS2 cleavage. Resolution of tropism across the respiratory tract is however more complex. Whilst, the regulation of ACE2 cleavage can readily explain attenuation in the lung, the counter explanation of augmented replication within the nasal epithelium appears is more complex and requires future investigations to determine if the solute carrier SLC6A20 may enable ACE2-TMPRSS2 cleavage resistance in this tissue. Given infection proceeds *in vivo* in these compartments in a TMPRSS2 dependent manner[3], we would support pools of ACE2 not to be subject to conditions that enable significant TMPRSS2-ACE2 cleavage and consequent attenuation on Omicron lineages.

Given the continued high level of spread of SARS CoV-2 globally and also the risk of co-circulation in other hosts, we need to continue phenotypic surveillance of variants to determine the consequences of continued viral evolution. Rapid detection of shifts in viral tissue tropism

and linkage to presentation of severity in the clinic are important in real-tracking many viruses including SARS CoV-2. However, to enable detection of tropism shifts, mechanistic resolution of the changing entry requirements is needed to distil this knowledge into entry screening platforms. Herein we not only determine the key change in entry requirements, but also outline assays that can readily determine if an emerging variant benefits from cleaved ACE2 usage and as such is on a trajectory towards or away from viral entry requirements that are now well known for pathogenic coronaviruses such as SARS-CoV-1 and early circulating clades on SARS-CoV-2. It is this latter rapid phenotypic surveillance of potential variants or ACE2 using coronaviruses that maybe key in identifying those which have higher clinical severity scores or tissue specific clinical manifestations such as lung related pneumonia. Furthermore, the observations herein provide the mechanistic foundation that can lead to alternate animal models (transgenic mice with TMPRSS2 resistant ACE2) to pragmatically use with Omicron lineages. This work further highlights the need to understand ACE2 pools at greater resolution and furthermore determine how ACE2's role as a solute carrier protein chaperone maybe driving evolution in SARS CoV-2's entry requirements. At a minimum, this work enables platforms *in vitro* that can increase sensitivity of SARS CoV-2 isolation, detection and phenotypic monitoring for not only pre-Omicron and past Omicron lineages but more importantly emerging Omicron variants. The latter alone will have significant impact in diagnostics and future surveillance and management of this pandemic virus.

Methods

Cell culture

HEK293T cells (thermo Fisher, R70007), HEK293T derivatives including HAT-24 [19], VeroE6-T1 (CellBank Australia, JCRB1819), VeroE6-T2 [21], VeroE6-T2-ACE2 and VeroE6-T2-NC-ACE2 were cultured in Dulbecco's Modified Eagle Medium (DMEM; Gibco, 11995073) with 10% fetal bovine serum (FBS) (Sigma; F7524). HEK293T-TetOne-ACE2 cells were cultured in DMEM with 10% fetal bovine serum (FBS) with 0.05µg/mL puromycin (Sigma; P8833). VeroE6 cells (ATCC CRL-1586) were cultured in Minimum Essential Medium (Gibco) with 10% FBS, 5% penicillin-streptomycin (Gibco; 15140122) and 1% L-glutamine (insert ref number). Calu3 cells were maintained in DMEM/F12 media (Gibco;12634010) supplemented with 1% MEM non essential amino acids (Sigma, M7145), 1% Glutamax (Gibco; 35050061) and 10% FBS. All cells used herein were only cultured and used within a range of 20 passages.

Generation of stable cell lines:

For generating VeroE6-T2 cells that stably express non-cleavable ACE2, expression plasmid pRRLsinPPT.CMV.GFP.WPRE was first modified to carry a multiple cloning site (MCS) at the 3' end of GFP open reading frame (ORF) using Age1 and Sal1 cut sites. The non-cleavable form of hACE2 (NC-ACE2) carrying mutations described previously by Heurich et al [31]was synthesised as a synthetic gBlock (IDT) and shuttled into the above plasmid using Xba1/Xho1 cut sites thus replacing the GFP ORF with NC-ACE2.

For generating HEK293T-TetOne-ACE2 cells, expression plasmid pLVX Tet-One Puro (Clontech) was modified to have a MCS at the 3'end of Tet responsive promoter TRE3GS using EcoR1/BamH1 cut sites. ACE2 ORF was amplified from pRRLsinPPT.CMV.ACE2.WPRE plasmid [19] and shuttled into pLVX Tet-One Puro-MCS expression plasmid using Not1/Xho1 sites to generate into pLVX Tet-One Puro-ACE2 plasmid. Plasmid sequences were validated by Nanopore Sequencing with the Rapid Barcoding Kit 96 (Oxford Nanopore Technologies) using manufacturers protocol. The sequencing data was exported as FASTQ files and analysed using Geneious Prime (v22.2). Open reading frames were then verified using Sanger Sequencing.

Cells expressing NC-ACE2 and inducible ACE2 were generated by lentiviral transductions as previously described[19]. Briefly, lentiviral particles expressing the above genes were produced by co-transfecting expression plasmids individually with a 2nd generation lentiviral packaging construct psPAX2 (courtesy of Dr Didier Trono through NIH AIDS repository) and VSVG plasmid pMD2.G (Addgene, 2259) in HEK293T producer cells using polyethyleneimine as previously described[52].Virus supernatant was collected 72 h post-transfection, pre-cleared of cellular debris and centrifuged at 28,000 × g for 90 min at 4 °C to generate concentrated virus stocks. Lentiviral transductions were then performed on VeroE6-T2 cells to generate VeroE6-T2-NC-ACE2 cells and Hek-293T cells to generate HEK293T-TetOne-ACE2. The expression of ACE2 in these cells was induced with 200ng/ml of Doxycycline (Sigma, D9891) as per manufacturer's instructions (ClonTech). Screening of clones was based on expression of high levels of ACE2 following Doxycycline in addition to being highly susceptible to the early clade SARS-CoV2 isolate A.2.2. HEK293T-TetOne-ACE2 cells were further modified to express hTMPRSS2[21] by lentiviral transductions to generate HEK293T-TetOne-ACE2-TMPRSS2 cells.

Viral isolation, propagation and titration from primary specimens

SARS-CoV2 variants were isolated from diagnostic respiratory specimens as previously described [23]. Briefly, specimens testing positive for SARS-CoV-2 (RT-qPCR, Seegene Allplex SARS-CoV-2) were sterile-filtered through 0.22 µm column-filters at 10,000 x *g* and serially diluted (1:3) on HAT-24 cells (10^4 cells/well in 96-well plates). Upon confirmation of cytopathic effect by light microscopy, 300 µL pooled culture supernatant and trypsinised cells from infected wells (passage 1) were added initially to a pellet of VeroE6-T2 cells (0.5×10^6 cells) for 30 minutes and then subsequently transferred to a 6-well plate (well with 2 mL of MEM2% final) and incubated for 48 h to 72 h (or until cytopathic effects had led to loss of >50% of the cell monolayer). The supernatant was cleared by centrifugation (2000 x *g* for 10 minutes), frozen at -80°C (passage 2), then thawed and titrated to determine median 50% Tissue Culture Infectious Dose ($TCID_{50}$/mL) on VeroE6-T2 cells according to the Spearman-Karber method [53]. Viral stocks used in this study correspond to passage 3 virus, which were generated by infecting VeroE6-T2 cells at MOI=0.025 and incubating for 24 h before collecting, clearing, and freezing the supernatant as above in 100ul aliquots. Sequence identity and integrity were confirmed for both passage 1 and passage 3 virus via whole-genome viral sequencing using an amplicon-based Illumina sequencing approach, as previously described [54]**.** The latter was also used in parallel for sequencing of primary nasopharyngeal swabs.

Virus titrations were carried out by serially diluting virus stocks (1:5) in MEM-2%FBS, mixing with cells initially in suspension at 5×10^3 cells/well in 384-well plates and then further incubating for 72 h. The cells were then stained live with 5% v/v nuclear dye (Invitrogen, R37605) and whole-well nuclei counts were determined with an IN Cell Analyzer 2500HS high-content microscope and IN Carta analysis software (Cytiva, USA). Data was normalized to generate sigmoidal dose–response curves (average counts for mock-infected controls = 100%, and average counts for highest viral concentration = 0%) and median Virus Effective (VE_{50}) values were obtained with GraphPad Prism software [23]. To assess the TMPRSS2 usage of the virus isolates, titrations on VeroE6-T2 were performed in the presence of saturating amounts of Nafamostat (20 µM). Titrations performed in parallel in equivalent volumes of DMSO served as controls and were used to calculate fold drops in VE_{50}."

ACE2 Affinofile Assay

Cells engineered with Doxycycline induced ACE2, were trypsinised and seeded as suspensions at 5×10^3 cells/well in 384-well plates. Cells were then exposed to Doxycycline for a minimum of four hours and at then each isolate was titered under each Doxycycline concentration. Cells were cultured for 72 h and then then stained live with 5% v/v nuclear dye. Sigmoidal curves using live nuclei counts were generated as described above and interpolated VE_{50} calculations were used to calculate viral titers to plot dose dependent changes at each ACE2/ Doxycycline concentration. To determine the influence of TMPRSS2, the same cell clone with Doxycycline induced ACE2 were lentivirally transduced with TMPRSS2 as described above and then subsequently cloned.

Phenotyping of ACE2 and TMPRSS2 on cell lines:

Cell lines (2.0 x 10^5 cells) were labelled with phycoerythrin-conjugated TMPRSS2 (Clone: S20014A, BioLegend) and AlexaFluor 647-conjugated ACE2 (Clone: 535919, R&D Systems)

for 30 mins on ice in the dark. Cells were washed once with FACS wash (phosphate buffered saline containing 2 mM EDTA and 1% heat-inactivated foetal bovine serum), prior to fixation with 1% paraformaldehyde (final) and acquisition by a BD LSRFortessa^{TM} flow cytometer (BD Biosciences). Flow cytometry analysis was performed using FlowJo analysis software (version 10.8.0, BD Biosciences).

Detection of Catalytic ACE2 in cell supernatants:
Soluble ACE2 activity in culture supernatants was measured as previously described [55].

Single resolution of known SARS CoV-2 entry factors with ACE2 associated solute protein carriers
Single cell RNAseq data from nasal [56] and ileum [57] were obtained from covid19cellatlas.org, while lung data [58] was obtained from GEO (GSE171524). These data were analysed with Seurat V4.3.0 as described previously [59]. Their accompanying metadata, which includes information such as sample ID, sample status, and cluster annotations (cell types), were added to Seurat objects using the "AddMetaData" function. Read counts were normalized using SCTransform, before reanalysis with the standard Seurat workflow of "RunPCA," "FindNeighbours," "FindClusters," and "RunUMAP." Cluster identities were assigned using published cluster annotations and plots were generated with "DimPlot", "Featureplot" and "DotPlot", to illustrate expression of *ACE2*, *TMPRSS2*, *SLC6A14*, *SLC6A19* and *SLC6A20*.

Statistical analysis:
Statistical analyses were performed using GraphPad Prism 9 (version 9.1.2, GraphPad software, USA). Sigmoidal dose response curves and interpolated IC50 values were determined using Sigmoidal, 4PL model of regression analysis in GraphPad Prism. For statistical significance, the datasets were initially assessed for Gaussian distribution, based on which further analysis was performed. For datasets that followed normal distribution, unpaired t-test was used to compare two groups. Details of statistical tests used for different data sets have also been provided in figure legends.

References

1 Lubel, J. S. *et al.* Angiotensin converting enzyme 2 (ACE2) activity in fetal calf serum: implications for cell culture research. *Cytotechnology* **58**, 119-126 (2008). https://doi.org:10.1007/s10616-009-9185-0

2 Yan, R. *et al.* Structural basis for the recognition of SARS-CoV-2 by full-length human ACE2. *Science* **367**, 1444-1448 (2020). https://doi.org:10.1126/science.abb2762

3 Metzdorf, K. *et al.* TMPRSS2 Is Essential for SARS-CoV-2 Beta and Omicron Infection. *Viruses* **15** (2023). https://doi.org:10.3390/v15020271

4 Halfmann, P. J. *et al.* SARS-CoV-2 Omicron virus causes attenuated disease in mice and hamsters. *Nature* **603**, 687-692 (2022). https://doi.org:10.1038/s41586-022-04441-6

5 Hui, K. P. Y. *et al.* SARS-CoV-2 Omicron variant replication in human bronchus and lung ex vivo. *Nature* **603**, 715-720 (2022). https://doi.org:10.1038/s41586-022-04479-6

6 Hui, K. P. Y. *et al.* Replication of SARS-CoV-2 Omicron BA.2 variant in ex vivo cultures of the human upper and lower respiratory tract. *EBioMedicine* **83**, 104232 (2022). https://doi.org:10.1016/j.ebiom.2022.104232

7 Zhu, Y. *et al.* Ancestral SARS-CoV-2, but not Omicron, replicates less efficiently in primary pediatric nasal epithelial cells. *PLoS Biol* **20**, e3001728 (2022). https://doi.org:10.1371/journal.pbio.3001728

8 Hoffmann, M. *et al.* SARS-CoV-2 Cell Entry Depends on ACE2 and TMPRSS2 and Is Blocked by a Clinically Proven Protease Inhibitor. *Cell* **181**, 271-280 e278 (2020). https://doi.org:10.1016/j.cell.2020.02.052

9 Korber, B. *et al.* Tracking Changes in SARS-CoV-2 Spike: Evidence that D614G Increases Infectivity of the COVID-19 Virus. *Cell* **182**, 812-827 e819 (2020). https://doi.org:10.1016/j.cell.2020.06.043

10 Zahradnik, J. *et al.* SARS-CoV-2 variant prediction and antiviral drug design are enabled by RBD in vitro evolution. *Nat Microbiol* **6**, 1188-1198 (2021). https://doi.org:10.1038/s41564-021-00954-4

11 Liu, Y. *et al.* The N501Y spike substitution enhances SARS-CoV-2 infection and transmission. *Nature* **602**, 294-299 (2022). https://doi.org:10.1038/s41586-021-04245-0

12 Bestle, D. *et al.* TMPRSS2 and furin are both essential for proteolytic activation of SARS-CoV-2 in human airway cells. *Life Sci Alliance* **3** (2020). https://doi.org:10.26508/lsa.202000786

13 Essalmani, R. *et al.* Distinctive Roles of Furin and TMPRSS2 in SARS-CoV-2 Infectivity. *J Virol* **96**, e0012822 (2022). https://doi.org:10.1128/jvi.00128-22

14 Zhang, J. *et al.* Membrane fusion and immune evasion by the spike protein of SARS-CoV-2 Delta variant. *Science* **374**, 1353-1360 (2021). https://doi.org:10.1126/science.abl9463

15 Liu, Y. *et al.* Delta spike P681R mutation enhances SARS-CoV-2 fitness over Alpha variant. *Cell Rep* **39**, 110829 (2022). https://doi.org:10.1016/j.celrep.2022.110829

16 Saito, A. *et al.* Enhanced fusogenicity and pathogenicity of SARS-CoV-2 Delta P681R mutation. *Nature* **602**, 300-306 (2022). https://doi.org:10.1038/s41586-021-04266-9

17 Willett, B. J. *et al.* Publisher Correction: SARS-CoV-2 Omicron is an immune escape variant with an altered cell entry pathway. *Nat Microbiol* **7**, 1709 (2022). https://doi.org:10.1038/s41564-022-01241-6

18 Carabelli, A. M. *et al.* SARS-CoV-2 variant biology: immune escape, transmission and fitness. *Nat Rev Microbiol* **21**, 162-177 (2023). https://doi.org:10.1038/s41579-022-00841-7

19 Aggarwal, A. *et al.* Platform for isolation and characterization of SARS-CoV-2 variants enables rapid characterization of Omicron in Australia. *Nat Microbiol* **7**, 896-908 (2022). https://doi.org:10.1038/s41564-022-01135-7

20 Matsuyama, S. *et al.* Enhanced isolation of SARS-CoV-2 by TMPRSS2-expressing cells. *Proc Natl Acad Sci U S A* **117**, 7001-7003 (2020). https://doi.org:10.1073/pnas.2002589117

21 Amarilla, A. A. *et al.* A versatile reverse genetics platform for SARS-CoV-2 and other positive-strand RNA viruses. *Nat Commun* **12**, 3431 (2021). https://doi.org:10.1038/s41467-021-23779-5

22 Tea, F. *et al.* SARS-CoV-2 neutralizing antibodies: Longevity, breadth, and evasion by emerging viral variants. *PLoS Med* **18**, e1003656 (2021). https://doi.org:10.1371/journal.pmed.1003656

23 Aggarwal, A. *et al.* SARS-CoV-2 Omicron BA.5: Evolving tropism and evasion of potent humoral responses and resistance to clinical immunotherapeutics relative to viral variants of concern. *EBioMedicine* **84**, 104270 (2022). https://doi.org:10.1016/j.ebiom.2022.104270

24 Meng, B. *et al.* Altered TMPRSS2 usage by SARS-CoV-2 Omicron impacts infectivity and fusogenicity. *Nature* **603**, 706-714 (2022). https://doi.org:10.1038/s41586-022-04474-x

25 Zhao, H. *et al.* SARS-CoV-2 Omicron variant shows less efficient replication and fusion activity when compared with Delta variant in TMPRSS2-expressed cells. *Emerg Microbes Infect* **11**, 277-283 (2022). https://doi.org:10.1080/22221751.2021.2023329

26 Akerman, A. *et al.* Emergence and antibody evasion of BQ, BA.2.75 and SARS-CoV-2 recombinant sub-lineages in the face of maturing antibody breadth at the population level. *EBioMedicine* **90**, 104545 (2023). https://doi.org:10.1016/j.ebiom.2023.104545

27 Yeung, M. L. *et al.* Soluble ACE2-mediated cell entry of SARS-CoV-2 via interaction with proteins related to the renin-angiotensin system. *Cell* **184**, 2212-2228 e2212 (2021). https://doi.org:10.1016/j.cell.2021.02.053

28 Chikere, K., Chou, T., Gorry, P. R. & Lee, B. Affinofile profiling: how efficiency of CD4/CCR5 usage impacts the biological and pathogenic phenotype of HIV. *Virology* **435**, 81-91 (2013). https://doi.org:10.1016/j.virol.2012.09.043

29 Yue, C. *et al.* ACE2 binding and antibody evasion in enhanced transmissibility of XBB.1.5. *Lancet Infect Dis* **23**, 278-280 (2023). https://doi.org:10.1016/S1473-3099(23)00010-5

30 Fountain, J. H., Kaur, J. & Lappin, S. L. in *StatPearls* (2023).

31 Heurich, A. *et al.* TMPRSS2 and ADAM17 cleave ACE2 differentially and only proteolysis by TMPRSS2 augments entry driven by the severe acute respiratory syndrome coronavirus spike protein. *J Virol* **88**, 1293-1307 (2014). https://doi.org:10.1128/JVI.02202-13

32 Shen, Y. *et al.* Structures of ACE2-SIT1 recognized by Omicron variants of SARS-CoV-2. *Cell Discov* **8**, 123 (2022). https://doi.org:10.1038/s41421-022-00488-x

33 Severe Covid, G. G. *et al.* Genomewide Association Study of Severe Covid-19 with Respiratory Failure. *N Engl J Med* **383**, 1522-1534 (2020). https://doi.org:10.1056/NEJMoa2020283

34 Stevens, B. R. TMPRSS2 and ADAM17 interactions with ACE2 complexed with SARS-CoV-2 and B0AT1 putatively in intestine, cardiomyocytes, and kidney. *bioRxiv* (2020). https://doi.org:https://doi.org/10.1101/2020.10.31.363473

35 Murhekar, M. V. *et al.* Seroprevalence of IgG antibodies against SARS-CoV-2 among the general population and healthcare workers in India, June-July 2021: A population-based cross-sectional study. *PLoS Med* **18**, e1003877 (2021). https://doi.org:10.1371/journal.pmed.1003877

36 Cele, S. *et al.* SARS-CoV-2 prolonged infection during advanced HIV disease evolves extensive immune escape. *Cell Host Microbe* **30**, 154-162 e155 (2022). https://doi.org:10.1016/j.chom.2022.01.005

37 Choi, B. *et al.* Persistence and Evolution of SARS-CoV-2 in an Immunocompromised Host. *N Engl J Med* **383**, 2291-2293 (2020). https://doi.org:10.1056/NEJMc2031364

38 Karim, S. S. A. & Karim, Q. A. Omicron SARS-CoV-2 variant: a new chapter in the COVID-19 pandemic. *Lancet* **398**, 2126-2128 (2021). https://doi.org:10.1016/S0140-6736(21)02758-6

39 Li, P., de Vries, A. C., Kamar, N., Peppelenbosch, M. P. & Pan, Q. Monitoring and managing SARS-CoV-2 evolution in immunocompromised populations. *Lancet Microbe* **3**, e325-e326 (2022). https://doi.org:10.1016/S2666-5247(22)00061-1

40 Willett, B. J. *et al.* SARS-CoV-2 Omicron is an immune escape variant with an altered cell entry pathway. *Nat Microbiol* **7**, 1161-1179 (2022). https://doi.org:10.1038/s41564-022-01143-7

41 Hirotsu, Y. *et al.* Lung tropism in hospitalized patients following infection with SARS-CoV-2 variants from D614G to Omicron BA.2. *Commun Med (Lond)* **3**, 32 (2023). https://doi.org:10.1038/s43856-023-00261-5

42 Zhang, Y. *et al.* SARS-CoV-2 spike L452R mutation increases Omicron variant fusogenicity and infectivity as well as host glycolysis. *Signal Transduct Target Ther* **7**, 76 (2022). https://doi.org:10.1038/s41392-022-00941-z

43 Qu, P. *et al.* Enhanced evasion of neutralizing antibody response by Omicron XBB.1.5, CH.1.1, and CA.3.1 variants. *Cell Rep* **42**, 112443 (2023). https://doi.org:10.1016/j.celrep.2023.112443

44 Iwata-Yoshikawa, N. *et al.* Essential role of TMPRSS2 in SARS-CoV-2 infection in murine airways. *Nat Commun* **13**, 6100 (2022). https://doi.org:10.1038/s41467-022-33911-8

45 Gong, J. *et al.* Genetic association and transcriptome integration identify contributing genes and tissues at cystic fibrosis modifier loci. *PLoS Genet* **15**, e1008007 (2019). https://doi.org:10.1371/journal.pgen.1008007

46 Di Paola, M. *et al.* SLC6A14 Is a Genetic Modifier of Cystic Fibrosis That Regulates Pseudomonas aeruginosa Attachment to Human Bronchial Epithelial Cells. *mBio* **8** (2017). https://doi.org:10.1128/mBio.02073-17

47 Bae, M. *et al.* SLC6A20 transporter: a novel regulator of brain glycine homeostasis and NMDAR function. *EMBO Mol Med* **13**, e12632 (2021). https://doi.org:10.15252/emmm.202012632

48 Rebendenne, A. *et al.* Bidirectional genome-wide CRISPR screens reveal host factors regulating SARS-CoV-2, MERS-CoV and seasonal HCoVs. *Nat Genet* **54**, 1090-1102 (2022). https://doi.org:10.1038/s41588-022-01110-2

49 Nieuwland, J. M. *et al.* Longitudinal positron emission tomography and postmortem analysis reveals widespread neuroinflammation in SARS-CoV-2 infected rhesus macaques. *J Neuroinflammation* **20**, 179 (2023). https://doi.org:10.1186/s12974-023-02857-z

50 Han, Y. *et al.* Identification of SARS-CoV-2 inhibitors using lung and colonic organoids. *Nature* **589**, 270-275 (2021). https://doi.org:10.1038/s41586-020-2901-9

51 Suarez-Farinas, M. *et al.* Intestinal Inflammation Modulates the Expression of ACE2 and TMPRSS2 and Potentially Overlaps With the Pathogenesis of SARS-CoV-2-

related Disease. *Gastroenterology* **160**, 287-301 e220 (2021). https://doi.org:10.1053/j.gastro.2020.09.029

52 Aggarwal, A. *et al.* Mobilization of HIV spread by diaphanous 2 dependent filopodia in infected dendritic cells. *PLoS Pathog* **8**, e1002762 (2012). https://doi.org:10.1371/journal.ppat.1002762

53 Ramakrishnan, M. A. Determination of 50% endpoint titer using a simple formula. *World J Virol* **5**, 85-86 (2016). https://doi.org:10.5501/wjv.v5.i2.85

54 Bull, R. A. *et al.* Analytical validity of nanopore sequencing for rapid SARS-CoV-2 genome analysis. *Nat Commun* **11**, 6272 (2020). https://doi.org:10.1038/s41467-020-20075-6

55 Lew, R. A. *et al.* Angiotensin-converting enzyme 2 catalytic activity in human plasma is masked by an endogenous inhibitor. *Exp Physiol* **93**, 685-693 (2008). https://doi.org:10.1113/expphysiol.2007.040352

56 Ziegler, C. G. K. *et al.* Impaired local intrinsic immunity to SARS-CoV-2 infection in severe COVID-19. *Cell* **184**, 4713-4733 e4722 (2021). https://doi.org:10.1016/j.cell.2021.07.023

57 Martin, J. C. *et al.* Single-Cell Analysis of Crohn's Disease Lesions Identifies a Pathogenic Cellular Module Associated with Resistance to Anti-TNF Therapy. *Cell* **178**, 1493-1508 e1420 (2019). https://doi.org:10.1016/j.cell.2019.08.008

58 Melms, J. C. *et al.* A molecular single-cell lung atlas of lethal COVID-19. *Nature* **595**, 114-119 (2021). https://doi.org:10.1038/s41586-021-03569-1

59 Loo, L. *et al.* Fibroblast-expressed LRRC15 is a receptor for SARS-CoV-2 spike and controls antiviral and antifibrotic transcriptional programs. *PLoS Biol* **21**, e3001967 (2023). https://doi.org:10.1371/journal.pbio.3001967

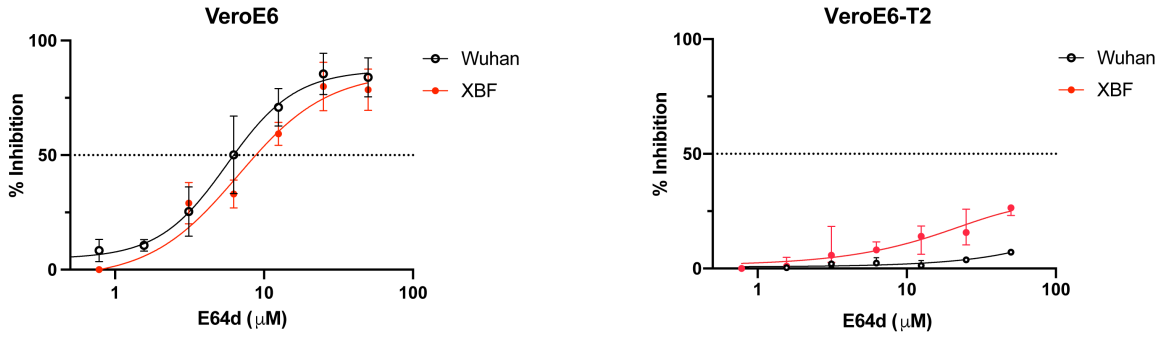

Supplementary Figure 1. Sensitivity of early and late SARS CoV-2 variants to E64D inhibition in VeroeE6 versus the VeroE6-T2 Cell line

A. Unmodified VeroE6s cells were exposed to increasing levels of the Cathepsin L Inhibitor E64D and then were infected with two isolates that represent early (A2.2.) versus contemporary (XBF) variants. B. Lack of inhibition of the pre-Omicron A2.2 versus the contemporary Omicron XBF in the VeroE6-T2 cell line.

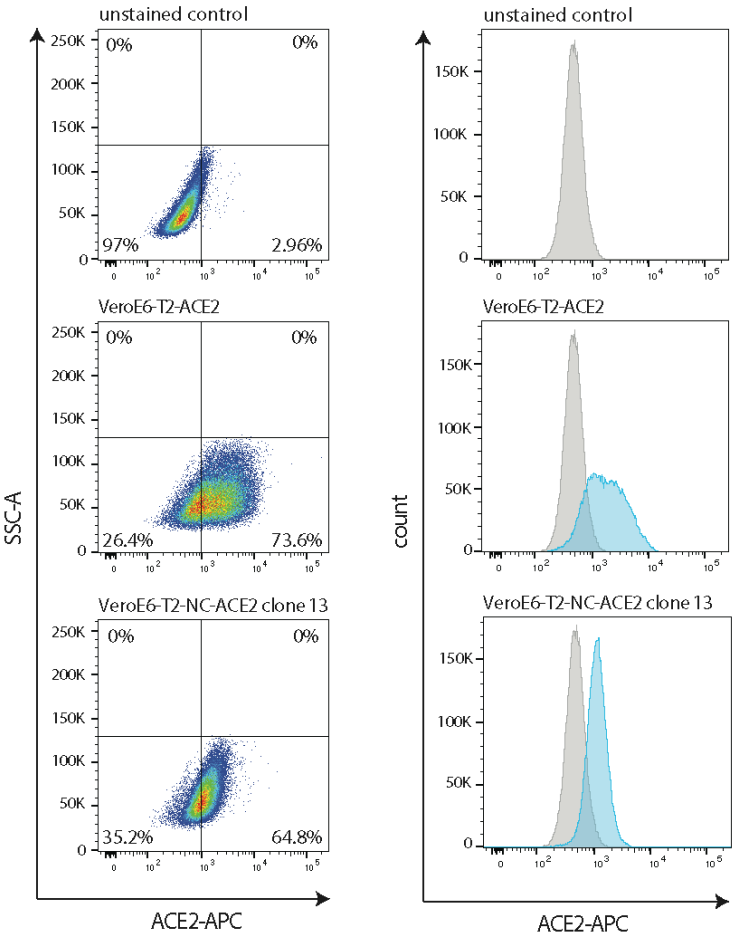

Supplementary Figure 2. ACE2 surface expression of the VeroE6-T2 cell line with WT ACE2 and TMPRSS2 resistant ACE2 (NC-ACE2).
Upper panel: Unstained control.
Middle panel: VeroE6-T2-ACE2
Lower panel: VeroE6-T2-NC ACE2 (TMPRSS2 resistant ACE2).